Growth of hexagonal quantum dots under preferential evaporation

Guido Schifani, Thomas Frisch, Jean-Noël Aqua

Patterns and dynamics: homage to Pierre Coullet / *Formes et dynamique : hommage à Pierre Coullet*

Growth of hexagonal quantum dots under preferential evaporation

Croissance de boîtes quantiques hexagonales sous évaporation préférentielle

Guido Schifani [a], Thomas Frisch [a], Jean-Noël Aqua [b],*

[a] *Université Côte d'Azur, CNRS, Institut de physique de Nice, Parc Valrose, 06108 Nice, France*
[b] *Sorbonne Université, CNRS, Institut des nanosciences de Paris, INSP, UMR 7588, 4, place Jussieu, 75005 Paris, France*

A B S T R A C T

We perform numerical simulations of hexagonal quantum dots of AlGaN semiconductors. We show that the competition between surface mass diffusion and evaporation rules the morphology of the quantum dots. The system displays three different behaviors: presence of separated islands without a wetting layer, islands dissolving into the wetting layer, or islands that do not evolve. The first behavior is of special interest because its optoelectrical properties are significantly improved in comparison with quantum dots with a wetting layer.

© 2019 Académie des sciences. Published by Elsevier Masson SAS. This is an open access article under the CC BY-NC-ND license (http://creativecommons.org/licenses/by-nc-nd/4.0/).

R É S U M É

Nous effectuons une simulation numérique des boîtes quantiques hexagonales de semiconducteurs AlGaN. Nous montrons que la compétition entre la diffusion de masse en surface et l'évaporation détermine la morphologie des boîtes quantiques. Le système montre trois comportements différents : des îlots séparés sans couche de mouillage, des îlots se dissolvant dans la couche de mouillage ou des îlots ne pouvant évoluer. Le premier comportement présente un intérêt particulier, car les propriétés optoélectriques sont considérablement améliorées par rapport aux boîtes quantiques avec une couche de mouillage.

© 2019 Académie des sciences. Published by Elsevier Masson SAS. This is an open access article under the CC BY-NC-ND license (http://creativecommons.org/licenses/by-nc-nd/4.0/).

* Corresponding author.
E-mail addresses: guido.schifani@inphyni.cnrs.fr (G. Schifani), thomas.frisch@inphyni.cnrs.fr (T. Frisch), aqua@insp.jussieu.fr (J.-N. Aqua).
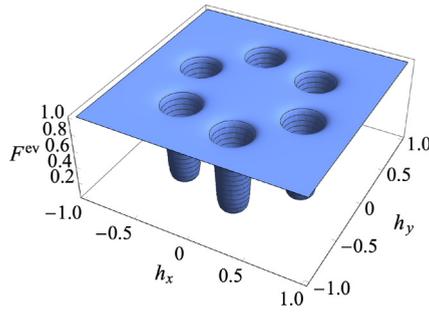
Fig. 1. Preferential evaporation following Eq. (2). The model involves six preferential evaporations, corresponding to the facets of the islands. For simplicity, we chose $F_{001}^{ev} = 1$, $p = 1/10$ and $\epsilon_e = 4$.

1. Introduction

The growth of self-organized quantum dots (QDs) has been widely studied due to their opto-electronic properties, from screen displays to single-photon emitters [1–3]. The development of a model that can predict the size, the shape, and the surface density of strained QDs remains a challenging task, since it involves the dynamic interplay of elasticity, capillarity, wetting, faceting, and alloying effects [4–14].

There are two essential phenomena for the morphological development of self-organized QDs. The first one is the development of the spatial instability, which selects a size. The second one is a coarsening phenomenon that broadens the size distribution of the islands. Coarsening is a general phenomenon in which the size of a pattern increases, whose description depends on transport mechanisms between QDs.

The formation of self-organized QDs results from the Stranski–Krastanow growth mode [15]. A thin semiconductor film is deposited and grows as a planar layer. Above a critical thickness, QDs emerge from this layer. This formation is explained by a partial relaxation of the elastic stress of the strained film, which is also submitted to capillarity and wetting effects. For low misfit [16,17], the instability is reminiscent of the Asaro–Tiller–Grinfeld (ATG) instability [18,5]. After its initial growth, the assembly of QDs undergoes coarsening, driven by the efficient elastic relaxation of the largest islands. The initially rough isotropic QDs (prepyramids) hence ripen and, as they display steep enough slopes, they transform into anisotropic QDs of various sizes, especially pyramids and domes [19].

We are interested in GaN QDs. It is observed experimentally that, after deposition of the semiconductor film, a preferential evaporation comes into play [20–22], which depends on the slope of the system and in which the wetting layer evaporates faster that the QDs. This effect drives the system to obtain QDs without a wetting layer, by which the optoelectrical properties improve significantly.

2. Continuum equation

We model the growth and evaporation of a semiconductor film by a continuum framework that describes surface mass diffusion. The film, lying in between $z = 0$ and the free surface $z = h(x, y, t)$, evolves following the mass conservation equation:

$$\frac{\partial h}{\partial t} = D \mathbf{\Delta} \mu + F^{dep} - F^{ev} \sqrt{1 + \nabla h^2} \tag{1}$$

where F^{dep}, F^{ev} correspond to the deposition and evaporation fluxes, while $\mu = \partial(\mathcal{F}^{el} + \mathcal{F}^{s})/\partial h$ is the chemical potential of the inhomogeneous surface, given by the functional derivative of the elastic and capillary free energies $\mathcal{F}^{el}$ and $\mathcal{F}^{s}$. We work with III–V semi-conductors, where F^{ev} is not negligible and depends on the local orientations $\boldsymbol{n}_0 = \{0, 0, 1\}$ and $\boldsymbol{n}_i = \frac{1}{2}\{\cos(i\frac{\pi}{3} + \frac{\pi}{4}), \sin(i\frac{\pi}{3} + \frac{\pi}{4}), \sqrt{3}\}$, $i = 1, \ldots 6$. We consider the following preferential evaporation function

$$F^{ev}(\boldsymbol{m}) = F_{001}^{ev} \left\{ 1 + \frac{1-p}{\pi} \sum_{j=1}^{6} \sum_{\sigma=0}^{1} (-1)^{\sigma} \arctan\left[\eta \left(||\boldsymbol{m} - \boldsymbol{m}_j|| - \frac{(-1)^{\sigma}}{\epsilon_e} ||\boldsymbol{m}_j|| \right) \right] \right\} \tag{2}$$

where F_{001}^{ev} is the evaporation of the substrate (001), $p = F_{113}^{ev}/F_{001}^{ev}$ the evaporation ratio of the facets and of the wetting layer, η and ϵ_e parameterize the dependence of evaporation on the local film orientation related to $\boldsymbol{m} = \{h_x, h_y\}$, while $\boldsymbol{m}_i = 2/\sqrt{3}\{n_{i,x}, n_{i,y}\}$. We plot in Fig. 1 the preferential evaporation for an hexagonal anisotropy. The surface energy $\mathcal{F}^{s} = \int \gamma(h, \boldsymbol{n}) \, \mathrm{d}^2 S$ depends on the surface energy as $\gamma = \gamma_f [1 + \gamma_a(\boldsymbol{n}) + \gamma_w(h)]$. Here γ_f is the energy of a thick-film, γ_a is the anisotropy energy and γ_w the wetting contribution. We consider again an hexagonal asymmetry for the surface energy anisotropy, described generically by
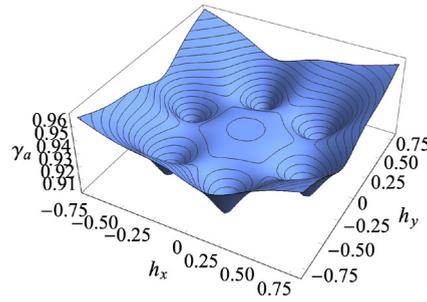
Fig. 2. Surface energy anisotropy given in Eq. (3). The preferential orientations represent the facets of the islands. The parameters for the facets are $A_\alpha = 0.07$, $\eta_\alpha = 4$, and $\epsilon_\alpha = 10^{-3}$ and for the flat orientation $A_0 = 0.2$, $\eta_0 = 10$, and $\epsilon_0 = 0.1$.

$$\gamma_{\mathrm{a}} = -\sum_{j=0}^{6} A_j \exp\left[-\eta_j \sqrt{1 - \boldsymbol{n} \cdot \boldsymbol{n}_j{}^2 + \epsilon_j}\right] \tag{3}$$

with the local normal $\boldsymbol{n} = \frac{1}{\sqrt{1+\nabla h^2}}\{-h_x, -h_y, 1\}$. The functional (3) leads with a small regularization ϵ_α, even with small anisotropy amplitudes A_α (Fig. 2). The wetting effect appears due to the interaction between the film/substrate interface and the film surface. In semiconductors, it generally has small variations, which we generically model as $\gamma_{\mathrm{w}}(h) = c_{\mathrm{w}} \exp(-h/\delta_w)$. Finally, elastic strain arises here due to the epitaxial misfit $m = (a^{\mathrm{f}} - a^{\mathrm{s}})/a^{\mathrm{s}}$ between the lattice parameters $a^{\mathrm{f/s}}$ of the film (f) and the substrate (s). We will use the elastic energy up to second order computed assuming the small-surface-slope approximation proposed in [19]. Its amplitude is given by the elastic energy density $\mathcal{E}_0 = Ym^2/(1-\nu)$, where Y and ν are Young's modulus and Poisson's ratio.

The characteristic length and time scales associated with the evolution equation (1) are $l_0 = \gamma_{\mathrm{f}}/2\,(1+\nu)\,\mathcal{E}_0$ and $t_0 = l_0^4/D\,\gamma_{\mathrm{f}}$ [19]. For example, in a GaN system, $\gamma_{\mathrm{f}} = 1.89$ J/m^2, and with its typical elastic parameters,[1] one finds $l_0 = 5.4$ nm for a GaN film on top of an Al$_{0.5}$Ga$_{0.5}$N substrate. The determination of t_0 is difficult, as the effective diffusion coefficient D is delicate to measure. We compare the experimental results with our numerical simulation in order to set a time scale $t_0 \simeq 1$ s.

3. Asaro–Tiller–Grinfeld instability

The system of a thin film semiconductor deposited on a semiconductor substrate presents a surface morphological instability. This instability was first studied within the framework of liquid epitaxy by Asaro and Tiller [18] and re-derived by Grinfeld [23]. The film diffuses in order to shape an undulated surface. This may only happen for film thicknesses above a characteristic value that we will derive subsequently. We emphasize that this instability develops thanks to surface diffusion driven by the strain resulting from the difference of the lattice sizes between the film and the substrate. The instability starts with an undulation that develops with time. This undulation takes place at the film free surface. If there is enough matter, the undulation transforms in bell-shaped islands.

We can solve the evolution Eq. (1) by considering a linear analysis where the film-free surface is decomposed into Fourier modes along x and y. The solution is an exponential growth $h(x, y, t) = h_0 + A\mathrm{e}^{\sigma t + \mathrm{i}k_x x + \mathrm{i}k_y y}$. σ reads:

$$\sigma = -\frac{1}{\gamma_{\mathrm{f}}}\left.\frac{\partial^2 \gamma(h, h_x, h_y)}{\partial h^2}\right|_{h=h_{\mathrm{c}}} k^2 + |k|^3 - \frac{\tilde{\gamma}(h_{\mathrm{c}}, h_x, h_y)}{\gamma_{\mathrm{f}}} k^4 \tag{4}$$

in dimensionless units. Here, the surface stiffness is defined as $\tilde{\gamma} = \gamma + \frac{\partial^2 \gamma}{\partial h_i \partial h_i}$.

For h_0 larger than some wetting critical thickness h_{c}, the growth rate presents positive values in a finite wavenumber interval and the instability develops as shown in Fig. 3. The critical thickness h_{c} is characterized by $\sigma = 0$ and $\partial\sigma/\partial k = 0$:

$$h_{\mathrm{c}} = \delta_w \ln(4\,c_{\mathrm{w}}/\delta_{\mathrm{w}}) \tag{5}$$

4. Hexagonal quantum dots

We present here numerical simulations of a system without preferential evaporation, in which the initial condition is a constant height $h_0 > h_{\mathrm{c}}$ plus a small random perturbation. In order to test our model with an hexagonal symmetry of the surface energy anisotropy, we study the effect of different parameters in order to have the best ones. We consider two initial heights $h_0 = 0.1$ and $h_0 = 0.35$ and, for each initial height, we vary the strength of the flat orientation n_0 given in Eq. (3).

---

[1] We used $Y = 300$ GPa, $\nu = 0.20$, $a_{\mathrm{GaN}} = 3.201$ Å, $a_{\mathrm{AlN}} = 3.126$ Å.
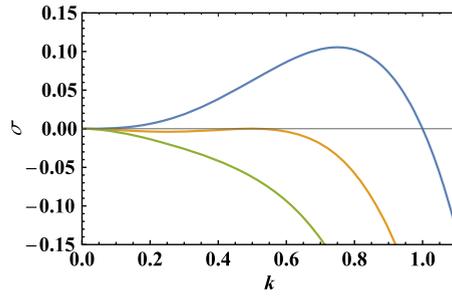
Fig. 3. Growth rate σ as a function of the wavenumber k given in Eq. (4). From top to bottom, the blue curve represents the growth rate for $h_0 > h_c$, the orange curve that for $h_0 = h_c$, and the green curve that for $h_0 < h_c$.
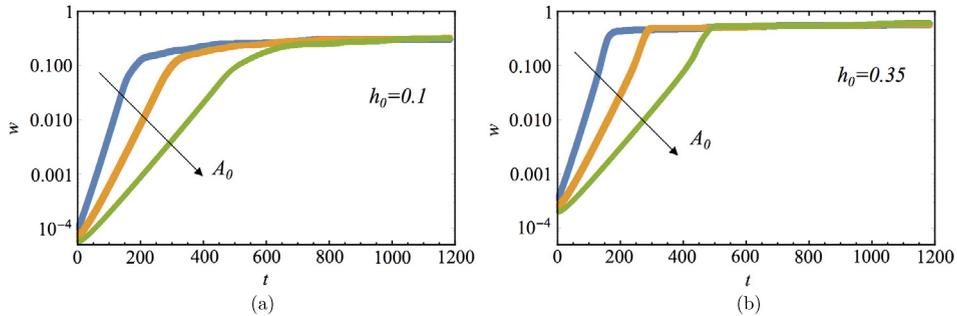

Fig. 4. Roughness as a function of time. The blue curve, the orange curve, and the green curve represent the numerical results for $A_0 = 0.2$, $A_0 = 0.35$, and $A_0 = 0.5$, respectively. (a) Initial height $h_0 = 0.1$ and (b) initial height $h_0 = 0.35$.
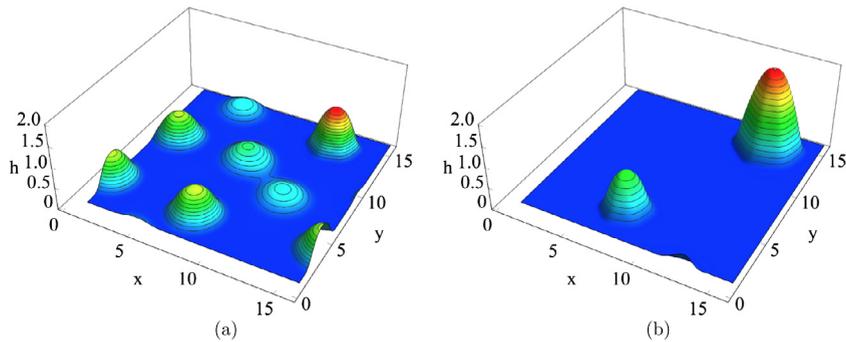

Fig. 5. Island profiles for different frame times. The colors range from blue to red depending on the value of the height, from the wetting layer height to the top of the island. (a) $t = 500$ and (b) $t = 1200$. The initial height is $h_0 = 0.1$.

We plot in Fig. 4 the roughness $w = \sqrt{<h^2> - <h>^2}$ as a function of time. We notice that the instability with a bigger initial height h_0 develops faster than the one with a small initial height. This feature is explained by the decrease of wetting interactions for large heights h. The wetting effect flattens the system and competes with the elasticity that drives the growth of islands. So, if the wetting interactions are stronger, the instability will take more time to develop. A similar behavior happens with the strength of the flat orientation (001) A_0. For systems in which the flat orientation is favorable, the development of the islands takes more time. As the flat orientation becomes a deeper local minimum, the system takes more time to go from small slopes to the facets' preferential orientation.

We plot in Fig. 5 and 6 QDs profiles for different times where the anisotropy strength $A_0 = 0.1$ and the height is $h_0 = 0.1$ and $h_0 = 0.35$, respectively. We can see that during coarsening, different shapes are encountered (truncated-elongated pyramids), but it depends on the total mass.

5. Preferential evaporation

We now study the evolution of the system in the presence of evaporation. Indeed, one characteristics of the III–V systems under study is the lower bounding on the surface, which leads to a significant evaporation during annealing. We take this extra-effect into account and, in addition, we consider anisotropic evaporation, as one knows that the facets evaporate at different speeds.
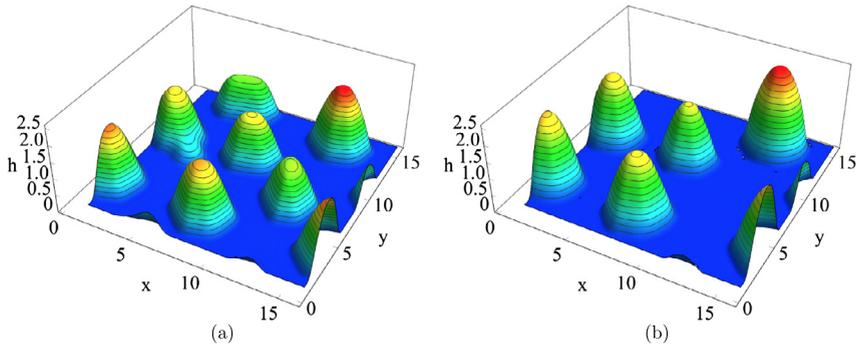
Fig. 6. Island profiles for different frame times. The colors range from blue to red depending on the value of the height, from the wetting layer height to the top of the island. (a) $t = 500$ and (b) $t = 1200$. The initial height is $h_0 = 0.35$.
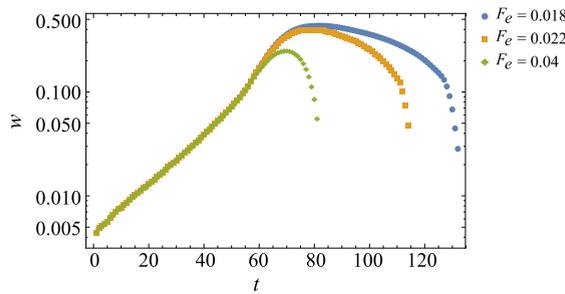

Fig. 7. Roughness as a function of the time, for three different values of the evaporation flux F_{001}^{ev}. The green rhombus are for $F_{001}^{ev} = 0.04$, the orange squares are for $F_{001}^{ev} = 0.022$, and the blue disks are for $F_{001}^{ev} = 0.018$. The initial height is $h_0 = 1.75$.

Our investigation concerns then the long-time dynamics of the system during long enough annealing/evaporation. We perform numerical simulations of Eq. (1) for the preferential evaporation given by Eq. (2): it will compete with the surface diffusion in the coarsening dynamics. When evaporation is high enough, the islands do not have time to appear before the entire system is evaporated, because surface diffusion is slower than evaporation. When evaporation is moderate/low, two behaviors can be met. The first behavior is when islands develop but, as the mass evaporates, the island dissolves in the wetting layer as, when the initial height is lower than h_c, the islands cannot develop. The second possible behavior occurs when evaporation is preferential, in which case the wetting layer vanishes, while islands remain in the system, keeping their shape. As the morphology is a result of the system's dynamics, no preferential insight can be given a priori.

The initial condition for the system under study is composed of a constant height h_0 plus a random perturbation. In comparison with the simulations presented in the previous section, here we choose an initial height h_0 of the order of magnitude of the typical island heights, since the evaporation will decrease the mass of the system until the mass vanishes, and in order to let the instability develop, the system will evaporate a considerable amount of mass before instability develops. We also chose a weak surface stiffness for the (001) orientation, since the numerical simulations are faster, as we have shown previously.

We expect that, for big evaporation fluxes, the instability cannot develop, because evaporation will win against mass diffusion, and the instability would not evolve. On the contrary, if the evaporation flux is slow, mass diffusion would win against evaporation, and the system will vanish.

We plot in Fig. 7 the temporal evolution of the roughness $w = \sqrt{<h^2> - <h>^2}$ as a function of the time, for a system with three values of preferential evaporation F_{001}^{ev}. We observe that roughness first increases, before it starts to decrease until becoming negative. Once the islands have their pyramidal shape, the preferential evaporation effect is more quantitative and makes the roughness decrease.

5.1. Vanishing of the wetting layer

We now present the results concerning the vanishing of the wetting layer. We perform numerical simulations of Eq. (1) for an initial height $h_0 = 1.75$, varying the evaporation flux of the wetting layer F_{001}^{ev}. We let the system evolve, and when the wetting layer presents negative values, we stop the simulation. We plot in Fig. 8 the layer profile at the moment when the wetting layer is negative. We notice that the region where the wetting layer vanishes exhibit a small periodic behavior, yet unsettled.
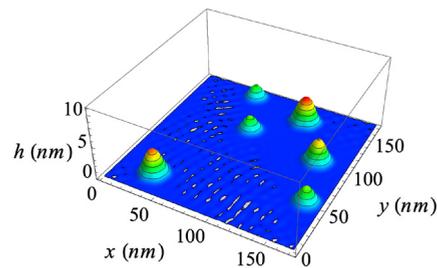
Fig. 8. Profile obtained by numerical simulation of Eq. (1), for the time when the wetting layer goes to negative values. The gray spots represent the negative values of the wetting layer. The evaporation flux is chosen to be $F_{001}^{ev} = 0.02$ and the initial height is $h_0 = 1.75$. Since the simulation is not realistic for negative values of the height, we stop the simulation here.

6. Conclusion

We study numerically a three-dimensional system, where the surface energy anisotropy presents a hexagonal symmetry, in order to favor hexagonal islands. We analyze the effects of the flat orientation and the effects of the initial height on the system.

– We find that a system with more mass presents faster coarsening. This behavior is rationalized by the wetting potential effect, which tries to flatten the system, and decays exponentially with the height, so that, when the initial height is bigger, the effect is weaker, and the islands evolve faster.
– A similar behavior occurs with a flat orientation in the surface energy anisotropy. If it is weak, a wetting layer is not preferential, so the system presents a high density of islands, and also, as this orientation is weak, coarsening will be faster.

We extend our model with a preferential evaporation. The experiments show that island facets evaporate slower than the wetting layer. Due to that, we add to our model a preferential evaporation. We show that, depending on the evaporation flux of the wetting layer, islands have time to develop or not. If islands develop, we show that, for certain times, the wetting layer vanishes.

References

[1] V.A. Shchukin, D. Bimberg, Spontaneous ordering of nanostructures on crystal surfaces, Rev. Mod. Phys. 71 (1999) 1125–1171.
[2] J. Stangl, V. Holý, G. Bauer, Structural properties of self-organized semiconductor nanostructures, Rev. Mod. Phys. 76 (2004) 725–783.
[3] J. Brault, S. Matta, T.-H. Ngo, D. Rosales, M. Leroux, B. Damilano, M. Al Khalfioui, F. Tendille, S. Chenot, P. De Mierry, J. Massies, B. Gil, Ultraviolet light emitting diodes using III–N quantum dots, Mater. Sci. Semicond. Process. 55 (2016) 95–101.
[4] B.J. Spencer, P.W. Voorhees, S.H. Davis, Morphological instability in epitaxially strained dislocation-free solid films, Phys. Rev. Lett. 67 (1991) 3696–3699.
[5] P. Müller, A. Saúl, Elastic effects on surface physics, Surf. Sci. Rep. 54 (5) (2004) 157–258.
[6] C.-H. Chiu, Z. Huang, Common features of nanostructure formation induced by the surface undulation on the Stranski–Krastanow systems, Appl. Phys. Lett. 89 (17) (2006) 171904.
[7] J.-N. Aqua, A. Gouyé, A. Ronda, T. Frisch, I. Berbezier, Interrupted self-organization of sige pyramids, Phys. Rev. Lett. 110 (2013) 096101.
[8] J.-N. Aqua, I. Berbezier, L. Favre, T. Frisch, A. Ronda, Growth and self-organization of SiGe nanostructures, Phys. Rep. 522 (2) (2013) 59–189.
[9] B.J. Spencer, J. Tersoff, Symmetry breaking in shape transitions of epitaxial quantum dots, Phys. Rev. B 87 (2013) 161301.
[10] C. Wei, B.J. Spencer, Asymmetric shape transitions of epitaxial quantum dots, Proc. R. Soc. A, Math. Phys. Eng. Sci. 472 (2190) (2016).
[11] F. Rovaris, R. Bergamaschini, F. Montalenti, Modeling the competition between elastic and plastic relaxation in semiconductor heteroepitaxy: from cyclic growth to flat films, Phys. Rev. B 94 (2016) 205304.
[12] C. Wei, B.J. Spencer, A Fokker–Planck reaction model for the epitaxial growth and shape transition of quantum dots, Proc. R. Soc. A, Math. Phys. Eng. Sci. 473 (2206) (2017).
[13] G. Schifani, T. Frisch, M. Argentina, J.-N. Aqua, Shape and coarsening dynamics of strained islands, Phys. Rev. E 94 (2016) 042808.
[14] G. Schifani, T. Frisch, M. Argentina, Equilibrium and dynamics of strained islands, Phys. Rev. E 97 (2018) 062805.
[15] I.N. Stranski, L. Krastanow, Zur Theorie der orientierten Ausscheidung von ionenkristallen Aufeinander, Monatsh. Chem. Verw. Tl. And. Wiss. 71 (1) (1937) 351–364.
[16] P. Sutter, M.G. Lagally, Nucleationless three-dimensional island formation in low-misfit heteroepitaxy, Phys. Rev. Lett. 84 (2000) 4637–4640.
[17] R.M. Tromp, F.M. Ross, M.C. Reuter, Instability-driven Si–Ge island growth, Phys. Rev. Lett. 84 (2000) 4641–4644.
[18] R.J. Asaro, W.A. Tiller, Interface morphology development during stress corrosion cracking: part I. Via surface diffusion, Metall. Trans. 3 (7) (1972) 1789–1796.
[19] J.-N. Aqua, T. Frisch, Influence of surface energy anisotropy on the dynamics of quantum dot growth, Phys. Rev. B 82 (2010) 085322.
[20] B. Damilano, J. Brault, J. Massies, Formation of gan quantum dots by molecular beam epitaxy using NH_3 as nitrogen source, J. Appl. Phys. 118 (2) (2015) 024304.
[21] J. Brault, S. Matta, T.-H. Ngo, M. Korytov, D. Rosales, B. Damilano, M. Leroux, P. Vennéguès, M. Al Khalfioui, A. Courville, O. Tottereau, J. Massies, B. Gil, Investigation of $Al_yGa_{1-y}N/Al_{0.5}Ga_{0.5}N$ quantum dot properties for the design of ultraviolet emitters, Jpn. J. Appl. Phys. 55 (5S) (2016) 05FG06.
[22] B. Damilano, S. Vézian, J. Brault, B. Alloing, J. Massies, Selective area sublimation: a simple top-down route for gan-based nanowire fabrication, Nano Lett. 16 (3) (2016) 1863–1868, PMID: 26885770.
[23] M.A. Grinfeld, Instability of the separation boundary between a nonhydrostatically stressed elastic body and a melt, Sov. Phys. Dokl. 31 (1986) 831.